Structure-Function–Based Quantitative Brain Image Analysis

Habib Zaidi, PhD, PD[a,b,*], Marie-Louise Montandon, PhD[a], Frédéric Assal, MD[c]

KEYWORDS

• Image fusion • PET-MRI • Quantification
• Neurodegenerative disease • Structural brain imaging
• Molecular brain imaging • PET • MRI

Modern functional brain mapping techniques, such as PET, single-photon emission CT (SPECT), functional MRI (fMRI), electroencephalography, magnetoencephalography, optical imaging, and neuroanatomic tools, have been used for assessing the functional organization of the human brain.[1,2] Through these techniques, neuroscience has progressed to a great extent in the understanding of the brain in health and disease. A comprehensive overview of these techniques and associated technologies is beyond the scope of this review, which focuses on recently developed high-resolution PET systems and dual-modality PET-MR units dedicated for brain imaging, particularly in the context of the assessment of dementia and related disorders.

The tendency in MR instrumentation development is to go for higher field strength to increase the signal-to-noise ratio in the resulting MRIs and as such achieving the highest possible field strength was strived for.[3] Although 3 T is becoming the state-of-the-art for clinical MRI, ultra–high-field MR systems are receiving considerable attention in preclinical[4] and clinical brain research. Several 7-T commercial scanners have become operational[5] whereas experimental 8- and 9.4-T scanners are under investigation.[6] Alternatively, the demand for functional, metabolic, and molecular imaging of the brain[7] has stimulated the development of dedicated high-resolution PET systems.[8,9]

To respond to the requirements of emerging clinical and research applications of correlated anatomic and functional brain imaging, several innovative developments in high performance standalone (PET and MRI) and dual-modality imaging instrumentation combining modalities have been proposed or are currently under design or testing. The development of combined PET-MR systems allowing simultaneous or sequential PET and MR brain imaging is an active research area.[10,11] This article discusses recent advances in multimodality brain imaging and the role of correlative fusion imaging and advanced quantitative imaging procedures in the clinical setting. Future opportunities and challenges facing the adoption of multimodality brain imaging also are addressed.

NEUROIMAGING IN THE DIAGNOSIS OF DEMENTIA AND RELATED DISORDERS

Neuroimaging is recommended by the 2001 practice parameters of the American Academy of

This work was supported by the Swiss National Science Foundation under grants SNSF 31003A-125246 and SNSF 33CM30-124114.

[a] Division of Nuclear Medicine, Geneva University Hospital, Geneva CH-1211, Switzerland
[b] Geneva Neuroscience Center, Geneva University, Geneva CH-1211, Switzerland
[c] Neurology, Department of Clinical Neurosciences, Geneva University Hospital, Geneva CH-1211, Switzerland
* Corresponding author. Division of Nuclear Medicine, Geneva University Hospital, Geneva CH-1211, Switzerland.
E-mail address: habib.zaidi@hcuge.ch

PET Clin 5 (2010) 155–168
doi:10.1016/j.cpet.2010.02.003

Neurology in the setting of neurodegenerative dementia and related disorders.[12] Structural brain imaging, preferably using MRI, not only rules out strokes, chronic subdural hematomas, cerebral neoplasms, or normal pressure hydrocephalus but also reveals characteristic patterns of regional atrophy that are commonly associated with clinical diagnosis.

In Alzheimer disease (AD), most investigators focused on reduced volume in the hippocampus or entorhinal cortex,[13–19] although its usefulness compared with clinical assessment alone has been questioned.[20] Other MRI-based studies reported atrophy in the superior parietal cortex and posterior cingulate/precuneus.[21–25] In frontotemporal dementia (FTD), atrophy is predominant in frontotemporal regions, depending on the clinical phenotype (ie, bilateral medial frontal or right frontal in the behavioral variant, left inferior frontal/left insula in the progressive nonfluent aphasia variant, and anterior temporal in the semantic dementia variant).[26–30]

Structural neuroimaging is less specific in the diagnosis of other non-AD neurodegenerative dementias and related disorders. Hippocampal atrophy is present in Lewy body dementia (LBD) and Parkinson disease dementia but to a lesser degree than in AD.[19,31–34] Predominant asymetric frontoparietal and midbrain atrophy is found, respectively, in corticobasal degeneration (CBD) and supranuclear palsy (PSP).[35–37]

Although not recommended by the 2001 practice parameters of the American Academy of Neurology, functional brain PET imaging using [^{18}F]-fluorodeoxyglucose (FDG)[38,39] and amyloid plaque tracers (mostly ^{11}C-labeled Pittsburgh compound B)[40] are increasingly used in the diagnosis of most common dementias.[41] The latter is still under investigation and not widely available for clinical use.

In AD, FDG-PET reveals hypometabolism in the precuneus/posterior cingulate and the lateral parietotemporal cortex[42–45] with sensitivity of 93% and specificity of 76%.[46] FDG-PET may be useful in distinguishing AD from FTD[47,48] or from vascular dementia.[49] Amyloid PET tracers may also help to discriminate early AD or mild cognitive impairment from normal controls,[50–52] and AD from FTD.[53,54] In FTD, FDG-PET supports the diagnosis but is not part of the Neary criteria.[55] It might be more sensitive than structural MRI in its early stages because hypometabolism in the frontotemporal regions may precede atrophy.[56,57]

In LBD, FDG-PET studies demonstrated parietotemporal and occipital hypoactivity[48,58–61] and low dopaminergic activity in the striatum using dopamine transporter imaging with ^{123}I-FP-CIT SPECT.[62,63] In CBD and PSP, when compared with each other or to controls, the former exhibited asymmetric hypometabolism in frontoparietal regions and lenticular nuclei whereas the latter exhibited asymmetric hypometabolism in frontal cortex, thalamus, and midbrain.[64–67] Nevertheless, currently available studies, often based on longitudinal changes over time, primarily evaluate structural and metabolic changes in groups of patients and are often inadequate to rely upon when evaluating individual patients.

Diagnosis of main dementias and related disorders at an early stage remains a challenge because of overlaps not only between main clinical diagnosis but also with normal aging.[68] Additional carefully designed clinical trials are needed to better validate structural MRI and FDG-PET (and other probes) as a diagnostic biomarker. Several studies have focused on correlated structural and functional data analysis involving coregistration of multimodality images. In AD, the hypoactivity in the posterior cingulate and in the precuneus remained significant after partial volume effect (PVE) correction using FDG-PET,[69–72] although other investigators suggested that the hypometabolism in the precuneus could at least be partly explained by the regional atrophy.[73] This discordance between atrophy and hypometabolism was present at the predementia stage where posterior cingulate/precuneus hypometabolism was associated with early memory deficits and left temporal hypometabolism marked the conversion to AD.[74] In LBD, FDG-PET findings report significant hypometabolism in the temporal, parietal, occipital, and frontal areas compared with those in the normal control group.[60]

OVERVIEW OF DEDICATED INSTRUMENTATION FOR MULTIMODALITY BRAIN IMAGING

Fig. 1 highlights the historical developments of brain PET imaging showing the improvement in image quality and spatial resolution as consequence of the noticeable improvement in PET instrumentation and image reconstruction techniques. As in whole-body imaging, high-detection sensitivity and spatial resolution and high-contrast and contrast resolution are the main concerns for imaging system design and constitute the basic requirements to achieving appropriate levels of image quality and quantitative accuracy. Thus, different dedicated brain PET designs have been and are still being developed in academic and corporate settings, with only a few units offered commercially. More recently, advanced versions of these technologies have begun to be used in

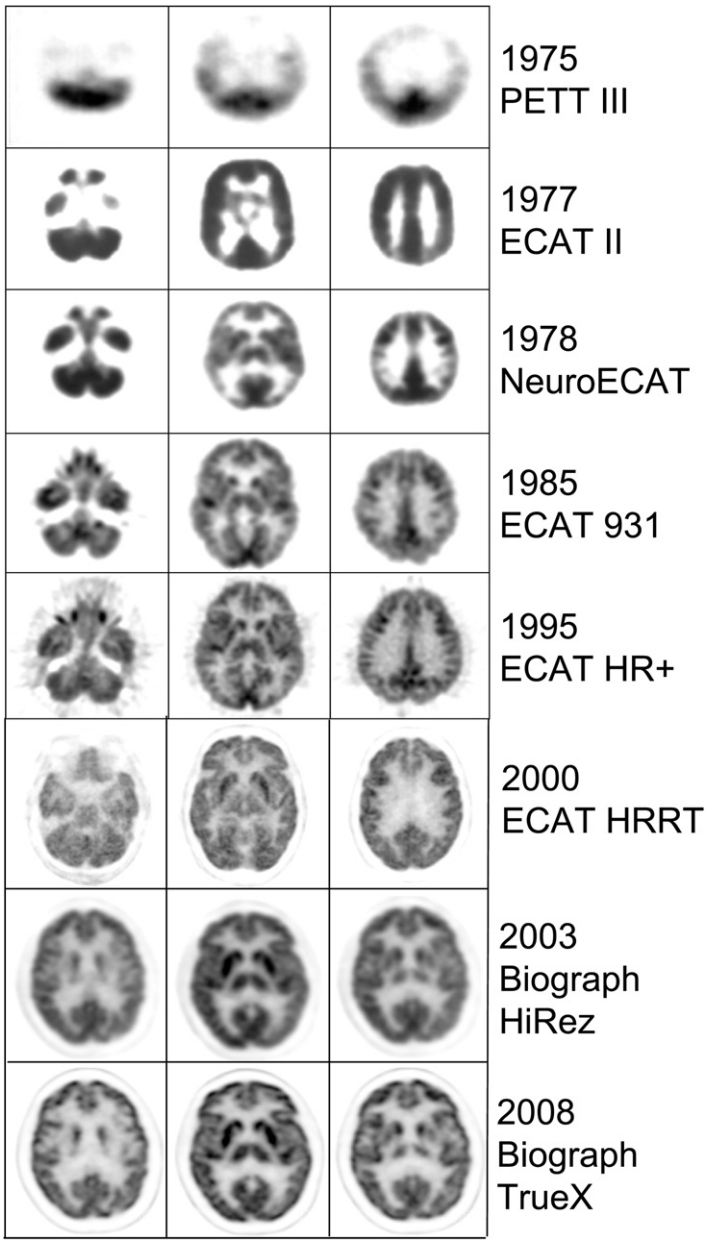

Fig. 1. Illustration of the significant improvement in clinical FDG brain PET image quality and spatial resolution resulting from the improvement in scanner performance for each generation during the past 3 decades. (*Reproduced from* Siemens Medical Solutions, Knoxville, TN; with permission.)

the study of brain function in myriad clinical and experimental settings.

To meet the objectives set by the molecular neuroimaging community, new-generation, high-resolution, 3D-only brain PET tomographs have been designed.[8,9] Current existing commercial brain PET technology (eg, the ECAT–high-resolution research tomograph [HRRT] developed by CTI-Siemens[75]) and other dedicated prototype designs, including G-PET[76] (developed at the University of Pennsylvania) and the Hamamatsu SHR-12000,[77] constitute state-of-the-art high resolution PET instrumentation dedicated for brain research. The HRRT consists of octagonal arrangements (42.4 cm face to face) of phoswich scintillator block detectors made of 2 layers of 64 small lutetium oxyorthosilicate (LSO) crystals (each $2.1 \times 2.1 \times 7.5$ mm^3) with 2 different decay times ($\Delta\tau \sim 7$ ns). The crystals (15 mm total active length) are oriented normal to the octagon sides, hence essentially

pointing in radial direction. The geometry of the G-PET brain scanner is similar to that of the HEAD PENN-PET[78] (developed at the University of Pennsylvania); however, the detector technology and electronic components have been redesigned to achieve improved performance. This scanner has a detector ring diameter of 42 cm and an axial field of view (FOV) of 25.6 cm and operates only in fully 3-D mode. It comprises 18,560 (320 × 58 array) 4 × 4 × 10 mm^3 gadolinium samarium oxalate (GSO) crystals coupled through a continuous light guide to 288 (36 × 8 array) 39-mm photomultiplier tubes in a hexagonal arrangement. Alternatively, the gantry and bed motions of the Hamamatsu SHR-12000 were designed specifically to allow subjects' scanning in lying, sitting, and standing postures, thus giving the possibility to research investigators of performing activation studies with high flexibility.[77] This scanner has a diameter of 50.8 cm and an axial FOV of 16.3 cm. It comprises 11,520 crystals arranged in 24 detector rings and 8 × 4 (2.8 × 6.55 × 30 mm^3 per crystal) bismuth germanate (BGO) detector blocks readout by compact position-sensitive PMTs. The scanner can be operated in 2-D or 3-D data acquisition modes when the interplane septa are retracted. Another design providing 4-layer depth-of-interaction (DOI) information, referred to as the jPET-D4 scanner (developed at the National Institute of Radiological Sciences, Chiba, Japan), was also developed with the aim of achieving high spatial resolution and high sensitivity by exploiting the DOI information obtained from multilayered thin crystals.[79] The system consists of 5 rings of 24 detector blocks each, each block consisting of 1024 GSO crystals (2.9 × 2.9 × 7.5 mm^3) arranged in 4 layers of 16 × 16 arrays.

Many conceptual designs developed specifically for small animal and nonhuman primates imaging could be applied equally well to high-resolution human brain imaging by increasing detector ring diameter and adapting the detector components accordingly. One such example is the clearPET Neuro scanner (developed by the Crystal Clear collaboration) dedicated for nonhuman primates imaging,[80] which uses a phoswich detector block combining 2 10-mm crystal layers of lutetium-based (LSO:Ce and LuYAP:Ce) scintillators segmented into 64 (8 × 8) detection elements with a cross section of 2 × 2 mm^2 coupled to multichannel photomultiplier tubes. The axial brain PET concept, which aimed to provide full 3-D reconstruction free of parallax errors with excellent spatial resolution over the total detector volume, was also recently suggested.[81] The detector modules consist of matrices of long axially oriented scintillation crystal bars, which are individually coupled on both ends to photodetectors. This design was improved by allowing the derivation of the axial coordinate from wavelength shifting plastic strips orthogonally interleaved between the crystal bars and readout by Geiger-mode avalanche photodiode arrays.[82]

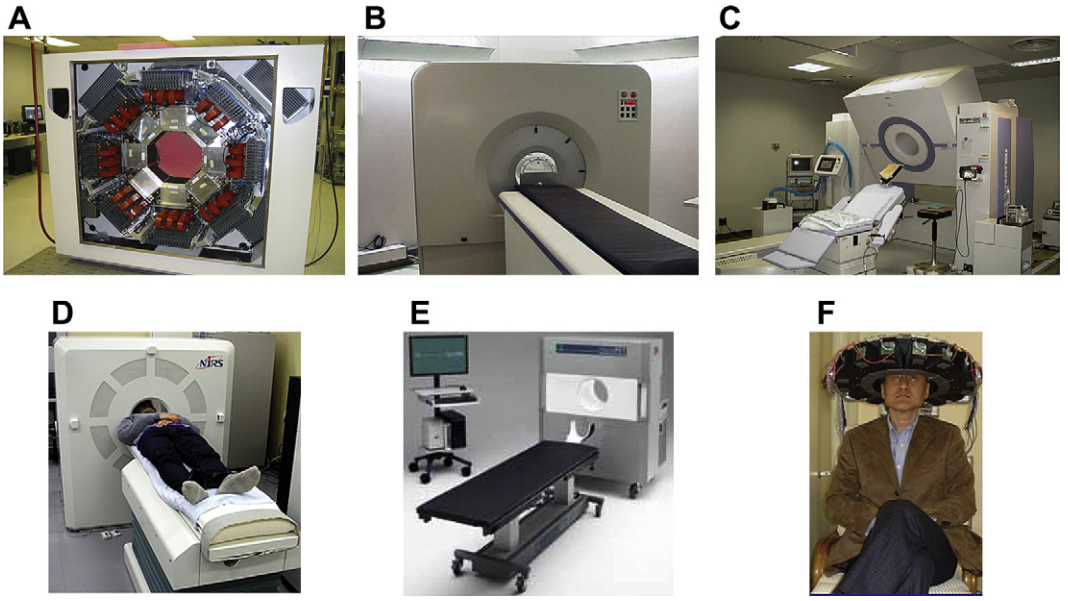

Fig. 2. Photographs of dedicated brain PET scanners showing (*A*) the HRRT camera based on LSO scintillation crystals and the phoswich concept, (*B*) the GSO-based PET (G-PET) camera, (*C*) the Hamamatsu SHR-12,000 PET scanner based on BGO detector blocks, (*D*) the jPET-D4 brain PET scanner, (*E*) the NeuroPET, and (*F*) the PET-Hat wearable PET system.

More recently, a novel platform, the NeuroPET (PhotoDetection Systems Inc, Boxboro, MA, USA), was proposed and made commercially available.[83] The Rat Conscious Animal PET (RATCAP; developed at Brookhaven National Laboratory, Upton, NY, USA)—a complete 3-D tomograph designed to image the brain of an awake rat,[84] like the PET-Hat (developed at Kobe City College of Technology, Kobe, Japan) wearable PET system—was also recently developed.[85] Because semiconductor detectors usually have higher-energy resolution compared with scintillation crystals. A new semiconductor-based brain PET scanner using a DOI detection system to reduce parallax error, thus achieving high spatial resolution and reduced scatter fraction, was proposed.[86] **Fig. 2** shows photographs of the some of the designs.

Few studies focused on the comparative assessment of the resulting spatial resolution and quantitative accuracy of brain imaging using dedicated high-resolution brain scanners with conventional whole-body designs. Although the Biograph 6 (Siemens Medical Solutions) PET-CT system was reported to have similar performance characteristics as the HR+ (Siemens Medical Solutions) for neuroimaging studies,[87] the higher pharmacokinetic parameter estimates obtained from the HRRT versus ECAT-HR+ (both manufactured by Siemens Medical Solutions) PET studies indicate improved HRRT PET quantification primarily due to a reduction in PVE.[88] This raises the issue of transfer of normal databases between PET systems with different performance characteristics for which some solutions have been suggested.

The availability of correlated functional (PET) and anatomic images (MRI) was exploited in a variety of clinical neurologic applications, including for cerebrovascular disorders, brain trauma, stroke, epilepsy, dementia, Parkinson disease, brain tumor, and mental disorders, such as depression, schizophrenia, and obsessive-compulsive disorders, as well as for localization of functional neuroactivation detected with PET. Software-based image registration has been successfully applied to neurologic studies (particularly for nonspecific tracers, such as FDG), where the skull provides a rigid structure that maintains the geometric relationship of structures within the brain and are now used routinely for clinical procedures at most institutions.[89,90] Although such methods are fully automated, their performance depends on many physiologic and technical aspects; further research is being conducted to evaluate their suitability in different clinical situations and their potential use in motion correction frequently encountered during lengthy PET scanning protocols.[91]

Contrary to hardware-based hybrid imaging combining PET and CT (PET-CT) systems in a single gantry to allow sequential scanning, which was successfully introduced in clinics in the beginning of this decade, combining PET with MR to allow simultaneous acquisition of spatially and temporally correlated PET-MR data sets is technically more challenging owing to the strong magnetic fields in the MR subsystem. The history of combined PET-MR dates back to the mid-1990s, however, before the advent of PET-CT.[92] Despite the challenges and technical difficulties, a clinical PET-MR prototype (BrainPET, Siemens Medical Solutions) dedicated for simultaneous PET-MR brain imaging was developed and installed in a few institutions for validation and testing.[10] **Fig. 3** illustrates the conceptual design and photograph of the integrated MR/PET scanner showing isocentric layering of MR head coil, PET detector ring, and MR magnet tunnel together with concurrently acquired clinical MR, PET, and fused MR/PET images. The system is being assessed in a clinical setting by exploiting the full potential of anatomic MRI in terms of high, soft tissue contrast sensitivity in addition to the many other possibilities offered by this modality, including blood oxygenation level–dependent imaging, fMRI, diffusion-weighted imaging, perfusion-weighted imaging, and diffusion tensor imaging.[93] A second sequential combined PET-MR system was also designed for molecular-genetic brain imaging by docking separate PET and MR systems together so that they share a common bed, which passes through the FOV of both cameras.[11] This is achieved by combining 2 high-end imaging devices, the HRRT and a 7-T MRI with submillimeter resolution.

QUANTITATIVE ANALYSIS OF BRAIN PET DATA

Subjective qualitative visual interpretation or semiquantitative analysis approaches involving operator-dependent and time-consuming manual volume-of-interest delineation techniques have been performed for decades and still are used routinely in many nuclear medicine departments. In the past few years, however, spatial normalization (or anatomic standardization) methods have become popular and widely available, thus allowing voxel-based analysis to be made. This has had an enormous contribution to PET activation studies and other studies involving the assessment of functional changes associated with neuropathology. Anatomic standardization allows the

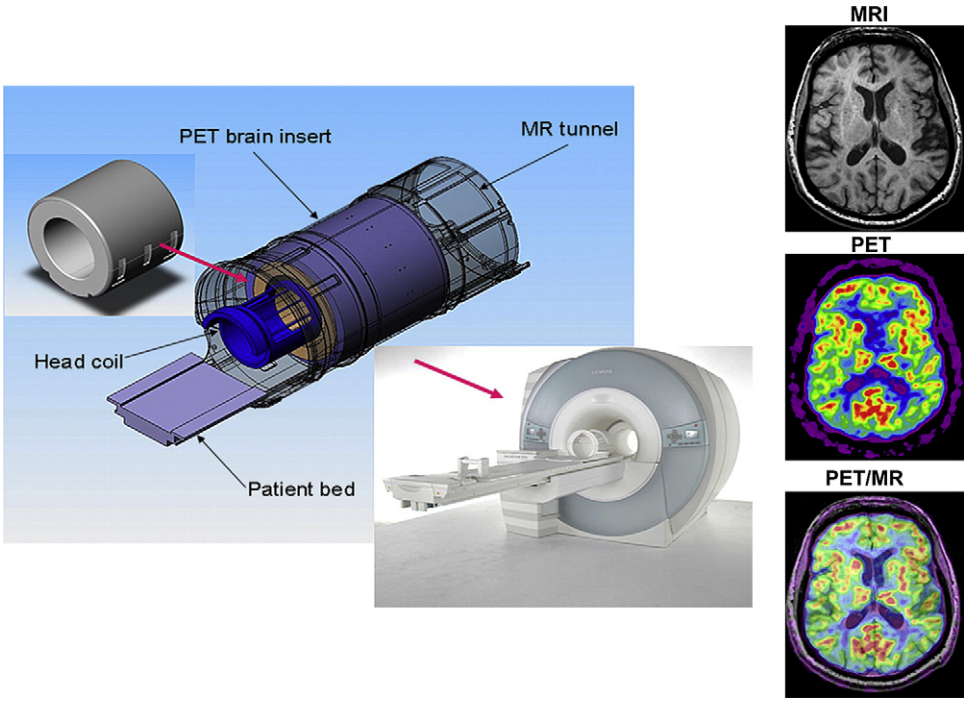

Fig. 3. Drawing and photograph of integrated MR/PET design showing isocentric layering of MR head coil, PET detector ring, and MR magnet tunnel (*left*). Simultaneously acquired MR, PET, and fused combined MRI/PET images of a 66-year-old man after intravenous injection of 370 MBq of FDG. Tracer distribution was recorded for 20 minutes at steady state after 120 minutes (*right*). (*Adapted and reprinted from* Schlemmer HP, Pichler BJ, Schmand M, et al. Simultaneous MR/PET imaging of the human brain: feasibility study. Radiology 2008;248:1028–35; with permission.)

transformation of brain images of individual subjects into a standard coordinate system, such as the stereotactic coordinate system proposed by Talairach and Tournoux.[94] Several methods for spatial normalization of brain images have been reported in the scientific literature, including Human Brain Atlas,[95] Statistical Parametric Mapping (SPM) software package (Wellcome Trust Centre for Neuroimaging, UCL Institute of Neurology, University College London, London, United Kingdom),[96] and 3D Stereotactic-Surface Projections (SSP) method developed by Minoshima and colleagues.[97]

The Human Brain Atlas uses morphologic information provided by PET-registered MRI.[95] The accuracy of the method is limited, however, by the precision that can be achieved by the coregistration procedure used to realign PET and MRI. SPM is among the state-of-the-art packages for statistical analysis of neuroimaging data including PET, SPECT, and fMRI. It is well documented, freely available, technically supported by well-established brain imaging centers,[96] and widely used by the neuroimaging community. The technique relies on morphologic images for the transformation into a standard coordinate system and has been extensively used to distinguish which structures of the brain are significantly activated by a neuroactivation task for a group of subjects or to identify which areas of the brain present with significant differences in metabolism (or cerebral blood flow) when comparing patient images with those of healthy volunteers. The steps involved in the statistical analysis of brain images include (1) spatial normalization of brain images into a standard stereotactic space for subsequent voxel-based analyses, (2) gaussian smoothing to correct for interindividual differences in underlying brain structures and allow the application of the general linear model approach for consecutive statistical analysis, and (2) the construction of statistical parametric maps.

Originally, SPM was developed for PET activation studies on healthy volunteers and was not intended for clinical application to diseased brains. For this reason, NEUROSTAT (Department of Internal Medicine, University of Michigan, Ann Arbor, MI, USA) was specially designed for statistical comparison between a normal database and diseased brains presenting with focal metabolic (perfusion) lesions.[97] The technique projects the cortical activity visualized in a 3-D volume image

onto the brain surface to generate a surface representation of the cortical activity distribution. This method was combined with the previously proposed standardization method by the same group, and the entire process referred to as 3D-SSP NEUROSTAT.

Among the commercial software packages, Brain Registration and Automated SPECT Semiquantification (BRASS) (Nuclear Diagnostics, Hägersted, Sweden) was designed for routine clinical brain SPECT and PET applications and allows 2 complementary quantitative comparisons of patient images with a 3-D reference atlas created from images of healthy volunteers: (1) a voxel-wise method and (2) an ROI-based regional analysis. The first can distinguish small defects but is sensitive to small registration errors and to the quality of the template whereas the second determines the mean and *z* scores within 3-D regions defined by a region map that has been matched to the template.[98] **Fig. 4** illustrates transverse views of an FDG-PET image of a patient with probable AD. The 3-D anatomically standardized brain PET template, the quantified defect for this patient, and the *z* score image obtained by the automated BRASS quantification procedure are also shown. PMOD (PMOD Technologies, Zürich, Switzerland) is another popular commercial multimodality medical imaging package based on a large FDG database of normal subjects acquired in a multicenter trial[99] for the discrimination between AD and controls. The PMOD Alzheimer discrimination analysis tool is an authorized implementation of this methodology. This method, although not approved for clinical use, may be used to analyze FDG-PET scans of patients with suspected AD for automatic discrimination analysis. The results point out brain areas with significant uptake

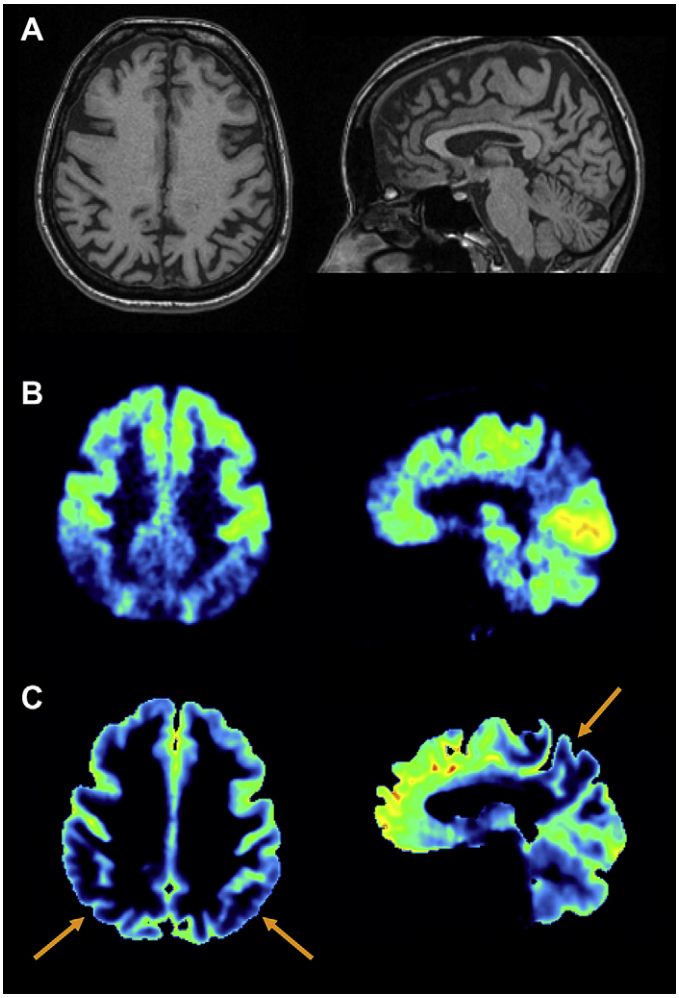

Fig. 4. Illustration of MRI-guided PVE correction impact in functional brain PET imaging showing for a patient with probable AD the original T1-weighted MRI (*A*) and PET images before (*B*) and after (*C*) PVE correction. The arrows point to evidence that the hypometabolism extends beyond the atrophy.

reduction ($P<.05$) and indicate a criterion of scan abnormality together with its error probability.

Several neuroimaging studies have been performed with the aim of evaluating the functional changes in healthy elderly brains and in patients with neurodegenerative diseases. The accurate measurement of tracer concentration, however, is corrupted by various physical degrading factors, including positron range,[100] limited spatial resolution and resulting PVE,[101] contribution from scattered photons,[102] photon attenuation,[103] patient motion,[104] and the image reconstruction algorithm.[105] Attenuation of photons degrades the visual quality and quantitative accuracy of PET images, thereby adversely affecting qualitative interpretation and quantitation of activity concentration. Accurate attenuation correction is, therefore, mandatory in quantitative PET image reconstruction and plays a pivotal role in clinical PET scanning protocols.[103] PVE leads to underestimation of the activity concentration in small structures of the brain (ie, with dimensions smaller than approximately 2–4 times the full width at half maximum of the scanner's point spread function). This problem is accentuated in the presence of brain atrophy, such as that encountered in AD, where this diluting effect is more pronounced. Compensation for PVE is then mandatory to offer the possibility of distinguishing the loss of radiotracer uptake due to PVE from the true metabolic values that decline with age or neuropathology.[69,106]

PVE compensation usually involves the following steps: (1) characterization of the point spread function of the imaging system, (2) characterization of the tissue components that participate in the uptake and metabolism of the tracer, and (3) characterization of the resolution effects in terms of correction factors or maps. PVE correction methods in brain PET may or may not require

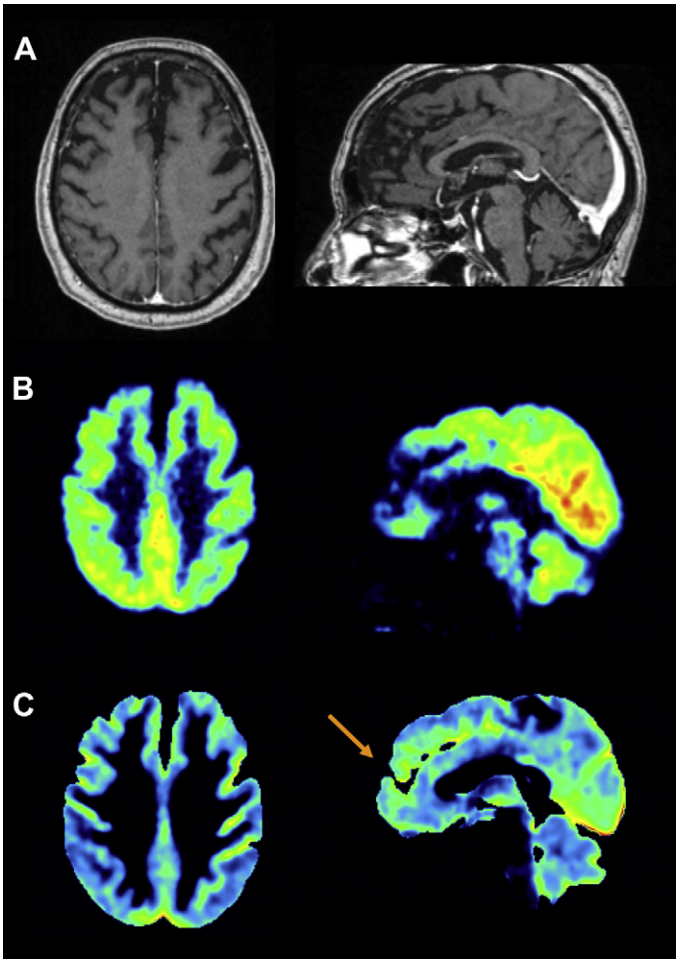

Fig. 5. Illustration of MRI-guided PVE correction impact in functional brain PET imaging showing for a patient with FTD the original T1-weighted MRI (*A*) and PET images before (*B*) and after (*C*) PVE correction. The arrow points to evidence that the hypometabolism matches the atrophy.

the availability of additional structural information from MRI of the same subject. MRI-guided PVE correction algorithms require as input segmented MRIs coregistered to PET data. It is assumed, therefore, that each segment of the activity distribution model represents a distinct and homogeneous activity distribution. Variants of this class of algorithms have been suggested and implemented successfully in a growing number of research studies.[101] Popular voxel-based approaches consider a heterogeneous distribution of the tracer uptake using a more realistic anatomic mask derived from MRI that makes the distinction between gray matter (GM) and white matter (WM) to account for WM activity contribution to measurements of GM activity concentration.[107,108]

The general principle of voxel-based MR-guided PVE correction in brain PET imaging involves the following steps[108]: first, the MRIs and PET images are spatially realigned, and then, the MRI is segmented into WM and GM. The latter is a popular research topic and a variety of image segmentation tools are available and have been used for this purpose.[109,110] The next step involves convolving the segmented WM and GM images by the PET scanner's spatial resolution modeled by a gaussian response function. The GM PET image is subsequently obtained by subtraction of the simulated WM PET image from the original PET image coregistered to MRI. The PVE corrected GM PET image is then obtained by dividing the GM PET image by the convolved GM MRI. A binary mask for GM is finally applied. Alternative approaches using deconvolution[111] and structural-functional synergetic multiresolution analysis[112,113] as well as those incorporated in statistical iterative reconstruction techniques,[114] which are more robust to coregistration errors, are being explored and exploited in research investigations.

CLINICAL IMPLICATIONS OF CORRELATED STRUCTURAL-FUNCTION–BASED QUANTITATIVE ANALYSIS

In recent years, efforts have been made to understand brain structure and function as they are related to aging and especially to neurodegenerative disorders. Multimodality brain imaging might

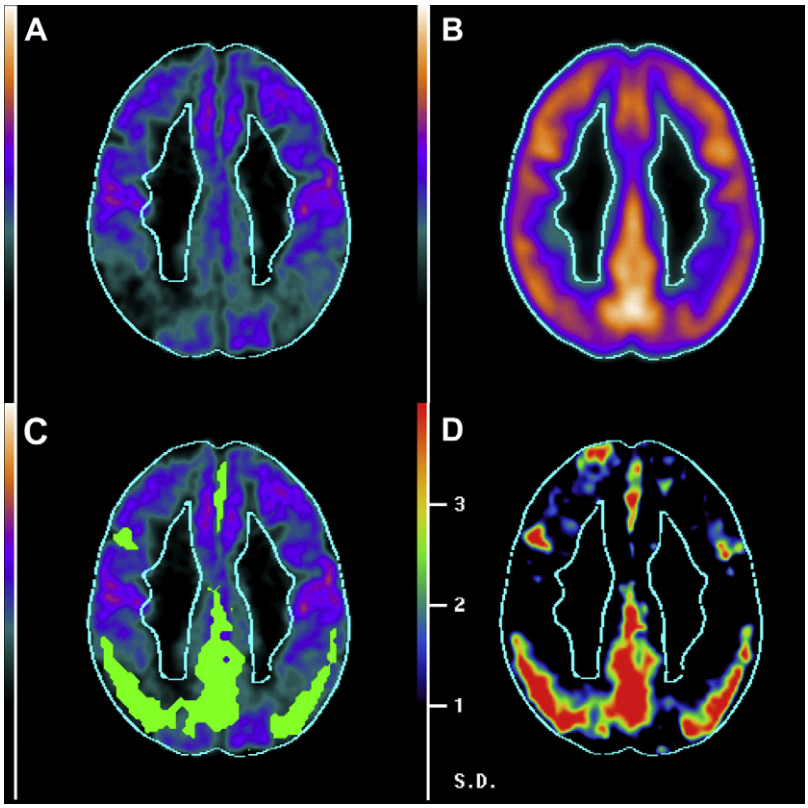

Fig. 6. Transverse views of the FDG-PET image of a patient with probable AD (*A*), the PET template (*B*), the quantified defect for this patient (*C*), and the *z*-score image (*D*), where the large red region indicates a region of significant hypometabolism. The isocontour indicates the external outline of the template.

be extremely important in the setting of future drugs that may help decrease disease progression. A main concern has been related to the PVE correction for cerebral metabolism in the atrophied brain, particularly in AD. **Figs. 5** and **6** illustrate the impact of PVE correction in functional FDG-PET brain imaging of a patient with probable AD and another patient with probable FTD, respectively.[115] The voxel-based MRI-guided PVE correction used follows the approach by Matsuda and colleagues[108] (described previously). In the early 1990s, it was already reported in the scientific literature that, although whole-brain metabolism is significantly reduced in AD patients compared with control subjects, this decrease loses its significance when metabolic rates are corrected for atrophy.[69,116] These findings stipulate that the hypometabolism of AD patients is related to atrophy whereas the remaining cerebral tissue has a metabolism comparable with that in controls. More recently, Bural and colleagues[117] reported on a new method using an MRI-based segmentation technique allowing the calculation of the standardized uptake values (SUV) in the GM, WM, and cerebrospinal fluid (CSF) in the corresponding PET images. This approach consists of the calculation of GM, WM, and CSF volumes from the segmented MRI. The next step involves the computation of the mean SUV representing the whole metabolic activity of the brain from the FDG-PET images. The whole-brain volume is calculated by summing the GM, WM, and CSF volumes, which is then used to calculate the global cerebral metabolic activity by multiplying the mean SUV by the total brain volume. Likewise, the global WM metabolic activity is estimated by multiplying the mean SUV for the WM by the WM volume. The CSF metabolic activity is assumed to be nil. The global GM metabolic activity is estimated by subtracting the global WM metabolic activity from that of the whole brain, which is then divided by the GM volume to provide an accurate estimate of the SUV for GM compartment.[118]

Correlative multimodality imaging of the brain might be a new tool not only to better diagnose neurodegenerative dementias and related disorders in differential and early diagnosis but also to better understand structure-function relationship.[119] It might be postulated that mismatch between hypometabolism and atrophy would imply different neuronal mechanisms than absence of mismatch in terms of disease progression, cognitive reserve, and neuronal plasticity. In addition, it might be hypothesized that mismatch might precede atrophy/structural changes or suggest hypometabolism-inducing factors, such as disconnection, loss of synapses, or protein deposition. On the contrary, regions where atrophy and hypometabolism are matched may benefit from compensatory mechanisms, suggesting neural plasticity. More importantly, different patterns might emerge in the course of the disease in the same individual in response to pharmacologic treatment, cognitive training, or compensatory mechanisms.

SUMMARY

Neurodegenerative dementias and related disorders produce significant alterations in the brain that may not be detectable with neuropsychological tests or with structural imaging, in the case of early or presymptomatic stage of a disease, because of overlaps with normal aging, or that may not be disease-specific (ie, the frontal variant of AD and FTD). FDG-PET, which is widely available is therefore ideally suited for monitoring cell/molecular events in early stages of neurodegenerative diseases, as well as in differential diagnosis and during pharmacologic therapy for monitoring of treatment response. During the past 2 decades, molecular brain imaging using PET and MR has advanced elegantly and steadily gained importance in the clinical and research arenas. Software- and hardware-based multimodality brain imaging has enabled the implementation of sophisticated anatomic-guided quantitative PET procedures that undoubtedly will revolutionize clinical diagnosis and offer unique capabilities for the clinical neuroimaging community and neuroscience researchers at large.

REFERENCES

1. Gilman S. Imaging the brain. First of two parts. N Engl J Med 1998;338:812–20.
2. Hammoud DA, Hoffman JM, Pomper MG. Molecular neuroimaging: from conventional to emerging techniques. Radiology 2007;245:21–42.
3. Hu X, Norris DG. Advances in high-field magnetic resonance imaging. Annu Rev Biomed Eng 2004; 6:157–84.
4. Cudalbu C, Mlynarik V, Xin L, et al. Comparison of T1 relaxation times of the neurochemical profile in rat brain at 9.4 tesla and 14.1 tesla. Magn Reson Med 2009;62:862–7.
5. van der Zwaag W, Francis S, Head K, et al. fMRI at 1.5, 3 and 7 T: characterising BOLD signal changes. Neuroimage 2009;47:1425–34.
6. Atkinson IC, Renteria L, Burd H, et al. Safety of human MRI at static fields above the FDA 8 T guideline: sodium imaging at 9.4 T does not affect vital signs or cognitive ability. J Magn Reson Imaging 2007;26:1222–7.

7. Jacobs AH, Li H, Winkeler A, et al. PET-based molecular imaging in neuroscience. Eur J Nucl Med Mol Imaging 2003;30:1051–65.
8. Zaidi H, Montandon M-L. The new challenges of brain PET imaging technology. Curr Med Imaging Rev 2006;2:3–13.
9. Sossi V. Cutting-edge brain imaging with positron emission tomography. PET Clin 2007;2:91–104.
10. Schlemmer HP, Pichler BJ, Schmand M, et al. Simultaneous MR/PET imaging of the human brain: feasibility study. Radiology 2008;248:1028–35.
11. Cho ZH, Son YD, Kim HK, et al. A fusion PET-MRI system with a high-resolution research tomograph-PET and ultra-high field 7.0 T-MRI for the molecular-genetic imaging of the brain. Proteomics 2008;8:1302–23.
12. Knopman DS, DeKosky ST, Cummings JL, et al. Practice parameter: diagnosis of dementia (an evidence-based review). Report of the Quality Standards Subcommittee of the American Academy of Neurology. Neurology 2001;56: 1143–53.
13. Devanand DP, Habeck CG, Tabert MH, et al. PET network abnormalities and cognitive decline in patients with mild cognitive impairment. Neuropsychopharmacology 2006;31:1327–34.
14. Jack CR Jr, Petersen RC, Xu YC, et al. Medial temporal atrophy on MRI in normal aging and very mild Alzheimer's disease. Neurology 1997; 49:786–94.
15. Sencakova D, Graff-Radford NR, Willis FB, et al. Hippocampal atrophy correlates with clinical features of Alzheimer disease in African Americans. Arch Neurol 2001;58:1593–7.
16. Vermersch P, Leys D, Scheltens P, et al. Visual rating of hippocampal atrophy: correlation with volumetry. J Neurol Neurosurg Psychiatry 1994; 57:1015.
17. Wahlund LO, Julin P, Johansson SE, et al. Visual rating and volumetry of the medial temporal lobe on magnetic resonance imaging in dementia: a comparative study. J Neurol Neurosurg Psychiatry 2000;69:630–5.
18. Bresciani L, Rossi R, Testa C, et al. Visual assessment of medial temporal atrophy on MR films in Alzheimer's disease: comparison with volumetry. Aging Clin Exp Res 2005;17:8–13.
19. Burton EJ, Barber R, Mukaetova-Ladinska EB, et al. Medial temporal lobe atrophy on MRI differentiates Alzheimer's disease from dementia with Lewy bodies and vascular cognitive impairment: a prospective study with pathological verification of diagnosis. Brain 2009;132:195–203.
20. Wahlund LO, Almkvist O, Blennow K, et al. Evidence-based evaluation of magnetic resonance imaging as a diagnostic tool in dementia workup. Top Magn Reson Imaging 2005;16:427–37.
21. Baron JC, Chetelat G, Desgranges B, et al. In vivo mapping of gray matter loss with voxel-based morphometry in mild Alzheimer's disease. Neuroimage 2001;14:298–309.
22. Frisoni GB, Testa C, Zorzan A, et al. Detection of grey matter loss in mild Alzheimer's disease with voxel based morphometry. J Neurol Neurosurg Psychiatry 2002;73:657–64.
23. Boxer AL, Rankin KP, Miller BL, et al. Cinguloparietal atrophy distinguishes Alzheimer disease from semantic dementia. Arch Neurol 2003;60:949–56.
24. Ishii K, Kawachi T, Sasaki H, et al. Voxel-based morphometric comparison between early- and late-onset mild Alzheimer's disease and assessment of diagnostic performance of z score images. AJNR Am J Neuroradiol 2005;26:333–40.
25. Whitwell JL, Shiung MM, Przybelski SA, et al. MRI patterns of atrophy associated with progression to AD in amnestic mild cognitive impairment. Neurology 2008;70:512–20.
26. Short RA, Broderick DF, Patton A, et al. Different patterns of magnetic resonance imaging atrophy for frontotemporal lobar degeneration syndromes. Arch Neurol 2005;62:1106–10.
27. Mummery CJ, Patterson K, Price CJ, et al. A voxel-based morphometry study of semantic dementia: relationship between temporal lobe atrophy and semantic memory. Ann Neurol 2000; 47:36–45.
28. Rosen HJ, Gorno-Tempini ML, Goldman WP, et al. Patterns of brain atrophy in frontotemporal dementia and semantic dementia. Neurology 2002;58:198–208.
29. CE Krueger, DL Dean, HJ Rosen, et al. Longitudinal rates of lobar atrophy in frontotemporal dementia, semantic dementia, and Alzheimer's disease. Alzheimer Dis Assoc Disord 2010;24:43–8.
30. Pereira JM, Williams GB, Acosta-Cabronero J, et al. Atrophy patterns in histologic vs clinical groupings of frontotemporal lobar degeneration. Neurology 2009;72:1653–60.
31. Middelkoop HA, van der Flier WM, Burton EJ, et al. Dementia with Lewy bodies and AD are not associated with occipital lobe atrophy on MRI. Neurology 2001;57:2117–20.
32. Tam CW, Burton EJ, McKeith IG, et al. Temporal lobe atrophy on MRI in Parkinson disease with dementia: a comparison with Alzheimer disease and dementia with Lewy bodies. Neurology 2005; 64:861–5.
33. Whitwell JL, Weigand SD, Shiung MM, et al. Focal atrophy in dementia with Lewy bodies on MRI: a distinct pattern from Alzheimer's disease. Brain 2007;130:708–19.
34. Kenny ER, Burton EJ, O'Brien JT. A volumetric magnetic resonance imaging study of entorhinal cortex volume in dementia with lewy bodies. A

comparison with Alzheimer's disease and Parkinson's disease with and without dementia. Dement Geriatr Cogn Disord 2008;26:218–25.
35. Boxer AL, Geschwind MD, Belfor N, et al. Patterns of brain atrophy that differentiate corticobasal degeneration syndrome from progressive supranuclear palsy. Arch Neurol 2006;63:81–6.
36. Josephs KA, Whitwell JL, Dickson DW, et al. Voxel-based morphometry in autopsy proven PSP and CBD. Neurobiol Aging 2008;29:280–9.
37. Koyama M, Yagishita A, Nakata Y, et al. Imaging of corticobasal degeneration syndrome. Neuroradiology 2007;49:905–12.
38. Varrone A, Asenbaum S, Vander Borght T, et al. EANM procedure guidelines for PET brain imaging using [18F]FDG, version 2. Eur J Nucl Med Mol Imaging 2009;36:2103–10.
39. Waxman AD, Herholz K, Lewis DH, et al. Society of Nuclear Medicine Procedure Guideline for FDG PET brain imaging. Available at: http://interactive.snm.org/index.cfm?PageID=772. Accessed January 30, 2010.
40. Klunk WE, Engler H, Nordberg A, et al. Imaging brain amyloid in Alzheimer's disease with Pittsburgh Compound-B. Ann Neurol 2004;55:306–19.
41. Cohen RM. The application of positron-emitting molecular imaging tracers in Alzheimer's disease. Mol Imaging Biol 2007;9:204–16.
42. Mosconi L, Nacmias B, Sorbi S, et al. Brain metabolic decreases related to the dose of the ApoE e4 allele in Alzheimer's disease. J Neurol Neurosurg Psychiatry 2004;75:370–6.
43. Nihashi T, Yatsuya H, Hayasaka K, et al. Direct comparison study between FDG-PET and IMP-SPECT for diagnosing Alzheimer's disease using 3D-SSP analysis in the same patients. Radiat Med 2007;25:255–62.
44. Del Sole A, Clerici F, Chiti A, et al. Individual cerebral metabolic deficits in Alzheimer's disease and amnestic mild cognitive impairment: an FDG PET study. Eur J Nucl Med Mol Imaging 2008;35:1357–66.
45. Minoshima S, Giordani B, Berent S, et al. Metabolic reduction in the posterior cingulate cortex in very early Alzheimer's disease. Ann Neurol 1997;42:85–94.
46. Silverman DH, Small GW, Chang CY, et al. Positron emission tomography in evaluation of dementia: regional brain metabolism and long-term outcome. JAMA 2001;286:2120–7.
47. Foster NL, Heidebrink JL, Clark CM, et al. FDG-PET improves accuracy in distinguishing frontotemporal dementia and Alzheimer's disease. Brain 2007;130:2616–35.
48. Ishii K, Imamura T, Sasaki M, et al. Regional cerebral glucose metabolism in dementia with Lewy bodies and Alzheimer's disease. Neurology 1998;51:125–30.
49. Kerrouche N, Herholz K, Mielke R, et al. 18FDG PET in vascular dementia: differentiation from Alzheimer's disease using voxel-based multivariate analysis. J Cereb Blood Flow Metab 2006;26:1213–21.
50. Edison P, Archer HA, Hinz R, et al. Amyloid, hypometabolism, and cognition in Alzheimer disease: an [11C]PIB and [18F]FDG PET study. Neurology 2007;68:501–8.
51. Jack CR Jr, Lowe VJ, Senjem ML, et al. 11C PiB and structural MRI provide complementary information in imaging of Alzheimer's disease and amnestic mild cognitive impairment. Brain 2008;131:665–80.
52. Nelissen N, Van Laere K, Thurfjell L, et al. Phase 1 study of the Pittsburgh compound B derivative 18F-flutemetamol in healthy volunteers and patients with probable Alzheimer disease. J Nucl Med 2009;50:1251–9.
53. Engler H, Santillo AF, Wang SX, et al. In vivo amyloid imaging with PET in frontotemporal dementia. Eur J Nucl Med Mol Imaging 2008;35:100–6.
54. Rabinovici GD, Furst AJ, O'Neil JP, et al. 11C-PIB PET imaging in Alzheimer disease and frontotemporal lobar degeneration. Neurology 2007;68:1205–12.
55. Neary D, Snowden JS, Gustafson L, et al. Frontotemporal lobar degeneration: a consensus on clinical diagnostic criteria. Neurology 1998;51:1546–54.
56. Ishii K, Sakamoto S, Sasaki M, et al. Cerebral glucose metabolism in patients with frontotemporal dementia. J Nucl Med 1998;39:1875–8.
57. Jeong Y, Song YM, Chung PW, et al. Correlation of ventricular asymmetry with metabolic asymmetry in frontotemporal dementia. J Neuroradiol 2005;32:247–54.
58. Mirzaei S, Knoll P, Koehn H, et al. Assessment of diffuse Lewy body disease by 2-[18F]fluoro-2-deoxy-D-glucose positron emission tomography (FDG PET). BMC Nucl Med 2003;3:1.
59. Gilman S, Koeppe RA, Little R, et al. Differentiation of Alzheimer's disease from dementia with Lewy bodies utilizing positron emission tomography with [18F]fluorodeoxyglucose and neuropsychological testing. Exp Neurol 2005;191(Suppl 1):S95–103.
60. Ishii K, Soma T, Kono AK, et al. Comparison of regional brain volume and glucose metabolism between patients with mild dementia with lewy bodies and those with mild Alzheimer's disease. J Nucl Med 2007;48:704–11.
61. Okamura N, Arai H, Higuchi M, et al. [18F]FDG-PET study in dementia with Lewy bodies and Alzheimer's disease. Prog Neuropsychopharmacol Biol Psychiatry 2001;25:447–56.

62. Ransmayr G, Seppi K, Donnemiller E, et al. Striatal dopamine transporter function in dementia with Lewy bodies and Parkinson's disease. Eur J Nucl Med 2001;28:1523–8.
63. McKeith I, O'Brien J, Walker Z, et al. Sensitivity and specificity of dopamine transporter imaging with 123I-FP-CIT SPECT in dementia with Lewy bodies: a phase III, multicentre study. Lancet Neurol 2007; 6:305–13.
64. Eckert T, Barnes A, Dhawan V, et al. FDG PET in the differential diagnosis of parkinsonian disorders. Neuroimage 2005;26:912–21.
65. Juh R, Pae CU, Kim TS, et al. Cerebral glucose metabolism in corticobasal degeneration comparison with progressive supranuclear palsy using statistical mapping analysis. Neurosci Lett 2005;383:22–7.
66. Coulier IM, de Vries JJ, Leenders KL. Is FDG-PET a useful tool in clinical practice for diagnosing corticobasal ganglionic degeneration? Mov Disord 2003;18:1175–8.
67. Garraux G, Salmon E, Peigneux P, et al. Voxel-based distribution of metabolic impairment in corticobasal degeneration. Mov Disord 2000;15: 894–904.
68. Chow TW, Binns MA, Freedman M, et al. Overlap in frontotemporal atrophy between normal aging and patients with frontotemporal dementias. Alzheimer Dis Assoc Disord 2008;22:327–35.
69. Alavi A, Newberg AB, Souder E, et al. Quantitative analysis of PET and MRI data in normal aging and Alzheimer's disease: atrophy weighted total brain metabolism and absolute whole brain metabolism as reliable discriminators. J Nucl Med 1993;34: 1681–7.
70. Chawluk J, Alavi A, Dann R, et al. Positron emission tomography in aging and dementia: effect of cerebral atrophy. J Nucl Med 1987;28:431–7.
71. Ibanez V, Pietrini P, Alexander GE, et al. Regional glucose metabolic abnormalities are not the result of atrophy in Alzheimer's disease. Neurology 1998;50:1585–93.
72. Chetelat G, Desgranges B, Landeau B, et al. Direct voxel-based comparison between grey matter hypometabolism and atrophy in Alzheimer's disease. Brain 2008;131:60–71.
73. He Y, Wang L, Zang Y, et al. Regional coherence changes in the early stages of Alzheimer's disease: a combined structural and resting-state functional MRI study. Neuroimage 2007;35:488–500.
74. Morbelli S, Piccardo A, Villavecchia G, et al. Mapping brain morphological and functional conversion patterns in amnestic MCI: a voxel-based MRI and FDG-PET study. Eur J Nucl Med Mol Imaging 2010;37:36–45.
75. Wienhard K, Schmand M, Casey ME, et al. The ECAT HRRT: performance and first clinical application of the new high resolution research tomograph. IEEE Trans Nucl Sci 2002;49:104–10.
76. Karp JS, Surti S, Daube-Witherspoon ME, et al. Performance of a brain PET camera based on anger-logic gadolinium oxyorthosilicate detectors. J Nucl Med 2003;44:1340–9.
77. Watanabe M, Shimizu K, Omura T, et al. A new high-resolution PET scanner dedicated to brain research. IEEE Trans Nucl Sci 2002;49:634–9.
78. Karp JS, Freifelder R, Geagan MJ, et al. Three-dimensional imaging characteristics of the HEAD PENN-PET scanner. J Nucl Med 1997;38:636–43.
79. Yamaya T, Hagiwara N, Obi T, et al. Preliminary resolution performance of the prototype system for a 4-layer DOI-PET scanner: jPET-D4. IEEE Trans Nucl Sci 2006;53:1123–8.
80. K Ziemons, R Achten, E Auffray, et al. The ClearPET™ neuro scanner: a dedicated LSO/LuYAP phoswich small animal PET scanner. In: Seibert JA, editor. IEEE Nuclear Science Symposium Conference Record, vol. 4. Rome (Italy), October 19–22, 2004. p. 2430–3.
81. Braem A, Chamizo Llatas M, Chesi E, et al. Feasibility of a novel design of high-resolution parallax-free Compton enhanced PET scanner dedicated to brain research. Phys Med Biol 2004;49:2547–62.
82. Braem A, Chesi E, Joram C, et al. Wavelength shifter strips and G-APD arrays for the read-out of the z-coordinate in axial PET modules. Nuclear Instruments and Methods in Physics Research Section A 2008;586:300–8.
83. Worstell W, Adler S, Domigan P, et al. Dynamic brain imaging with low injection dose using the NeuroPET [abstract]. J Nucl Med 2009;50:137P.
84. Vaska P, Woody CL, Schlyer DJ, et al. RatCAP: miniaturized head-mounted PET for conscious rodent brain imaging. IEEE Trans Nucl Sci 2004; 51:2718–22.
85. Yamamoto S, Honda M, Shimizu K, et al. Development of PET-Hat: Wearable PET system for brain research [abstract]. J Nucl Med 2009;50:1532.
86. Morimoto Y, Ueno Y, Tsuchiya K, et al. Performance of a prototype brain PET scanner based on semiconductor detectors. J Nucl Med 2008;49:122P [abstract].
87. Trebossen R, Comtat C, Brulon V, et al. Comparison of two commercial whole body PET systems based on LSO and BGO crystals respectively for brain imaging. Med Phys 2009;36:1399–409.
88. van Velden FHP, Kloet RW, van Berckel BNM, et al. HRRT versus HR+ human brain PET studies: an interscanner test-retest study. J Nucl Med 2009; 50:693–702.
89. Woods RP, Mazziotta JC, Cherry SR. MRI-PET registration with automated algorithm. J Comput Assist Tomogr 1993;17:536–46.

90. Pietrzyk U, Herholz K, Fink G, et al. An interactive technique for three-dimensional image registration: validation for PET, SPECT, MRI and CT brain studies. J Nucl Med 1994;35:2011–8.
91. Slomka P, Baum R. Multimodality image registration with software: state-of-the-art. Eur J Nucl Med Mol Imaging 2009;36:44–55.
92. Hammer BE, Christensen NL, Heil BG. Use of a magnetic field to increase the spatial resolution of positron emission tomography. Med Phys 1994; 21:1917–20.
93. Holdsworth SJ, Bammer R. Magnetic resonance imaging techniques: fMRI, DWI, and PWI. Semin Neurol 2008;28:395–406.
94. Talairach J, Tournoux P. Co-planar atlas of the human brain. New York: Thieme Medical Publishers; 1988.
95. Roland PE, Zilles K. Brain atlases—a new research tool. Trends Neurosci 1994;17:458–67.
96. Friston K, Ashburner J, Heather J, et al. Statistical parametric mapping. Available at: http://www.fil.ion.ucl.ac.uk/spm. Accessed February 10, 2010. The Wellcome Department of Cognitive Neurology, University College London. 1999.
97. Minoshima S, Koeppe RA, Frey KA, et al. Stereotactic PET atlas of the human brain: aid for visual interpretation of functional brain images. J Nucl Med 1994;35:949–54.
98. Slomka PJ, Radau P, Hurwitz GA, et al. Automated three-dimensional quantification of myocardial perfusion and brain SPECT. Comput Med Imaging Graph 2001;25:153–64.
99. Herholz K, Salmon E, Perani D, et al. Discrimination between Alzheimer dementia and controls by automated analysis of multicenter FDG PET. Neuroimage 2002;17:302–16.
100. Sanchez-Crespo A, Andreo P, Larsson SA. Positron flight in human tissues and its influence on PET image spatial resolution. Eur J Nucl Med Mol Imaging 2004;31:44–51.
101. Rousset O, Rahmim A, Alavi A, et al. Partial volume correction strategies in PET. PET Clin 2007;2:235–49.
102. Zaidi H, Montandon M-L. Scatter compensation techniques in PET. PET Clin 2007;2:219–34.
103. Zaidi H, Montandon M-L, Meikle S. Strategies for attenuation compensation in neurological PET studies. Neuroimage 2007;34:518–41.
104. Rahmim A, Rousset O, Zaidi H. Strategies for motion tracking and correction in PET. PET Clin 2007;2:251–66.
105. Reader AJ, Zaidi H. Advances in PET image reconstruction. PET Clin 2007;2:173–90.
106. Meltzer CC, Cantwell MN, Greer PJ, et al. Does cerebral blood flow decline in healthy aging? A PET study with partial-volume correction. J Nucl Med 2000;41:1842–8.
107. Muller-Gartner HW, Links JM, Prince JL, et al. Measurement of radiotracer concentration in brain gray matter using positron emission tomography: MRI-based correction for partial volume effects. J Cereb Blood Flow Metab 1992;12:571–83.
108. Matsuda H, Ohnishi T, Asada T, et al. Correction for partial-volume effects on brain perfusion SPECT in healthy men. J Nucl Med 2003;44:1243–52.
109. Meltzer CC, Kinahan PE, Greer PJ, et al. Comparative evaluation of MR-based partial-volume correction schemes for PET. J Nucl Med 1999;40:2053–65.
110. Zaidi H, Ruest T, Schoenahl F, et al. Comparative evaluation of statistical brain MR image segmentation algorithms and their impact on partial volume effect correction in PET. Neuroimage 2006;32: 1591–607.
111. Tohka J, Reilhac A. Deconvolution-based partial volume correction in Raclopride-PET and Monte Carlo comparison to MR-based method. Neuroimage 2008;39:1570–84.
112. Boussion N, Hatt M, Lamare F, et al. A multiresolution image based approach for correction of partial volume effects in emission tomography. Phys Med Biol 2006;51:1857–76.
113. Shidahara M, Tsoumpas C, Hammers A, et al. Functional and structural synergy for resolution recovery and partial volume correction in brain PET. Neuroimage 2009;44:340–8.
114. Baete K, Nuyts J, Laere KV, et al. Evaluation of anatomy based reconstruction for partial volume correction in brain FDG-PET. Neuroimage 2004; 23:305–17.
115. M Montandon, F Assal, O Ratib, et al. MRI-guided voxel-based partial volume effect correction in brain PET: assessment of the impact of 3 MR image segmentation algorithms. 15th Annual Meeting, Organization for Human Brain Mapping (HBM). San Francisco, June 18–23, 2009;47:365.
116. Kohn MI, Tanna NK, Herman GT, et al. Analysis of brain and cerebrospinal fluid volumes with MR imaging. Part I. Methods, reliability, and validation. Radiology 1991;178:115–22.
117. Bural GG, Zhuge Y, Torigian DA, et al. Partial volume correction and segmentation allows accurate measurement of SUV for the grey matter in the brain [abstract]. J Nucl Med 2006;47:9P.
118. Basu S, Zaidi H, Houseni M, et al. Novel quantitative techniques for assessing regional and global function and structure based on modern imaging modalities: implications for normal variation, aging and diseased states. Semin Nucl Med 2007;37: 223–39.
119. Zaidi H, Montandon M, Alavi A. The clinical role of fusion imaging using PET, CT and MRI. Magn Reson Imaging Clin N Am 2010;18:133–49.